narra j

Original Article

Cytoarchitectural changes in the developing cerebellar cortex of the *laggard* mutant mouse

Junaedy Yunus[1*], Tomiyoshi Setsu[2], Satoshi Kikkawa[2] and Toshio Terashima[3]

[1]Department of Anatomy, Faculty of Medicine, Public Health, and Nursing, Universitas Gadjah Mada, Yogyakarta, Indonesia; [2]Division of Structural Medicine and Anatomy, Department of Physiology and Cell Biology, Kobe University Graduate School of Medicine, Kobe, Japan; [3]Division of Developmental Neurobiology, Department of Physiology and Cell Biology, Kobe University Graduate School of Medicine, Kobe, Japan

*Corresponding author: junaedy_yunus@ugm.ac.id

Abstract

The *laggard* (*lag*) mutant mouse, which arises from a mutation in the *Kif14* gene, begins to exhibit ataxia and impaired growth after the first postnatal week and subsequently dies prematurely around two weeks of age. In this mutant mouse, the layered architecture of the cerebellar cortex, cerebral cortex, dentate gyrus, and olfactory bulb is disrupted at the cellular level. The aim of this study was to identify the effect of *Kif14* mutation on the development of the cerebellar cortex. Abnormalities in the cytoarchitectonics of the developing cerebellar cortex were assessed using hematoxylin-eosin (HE) staining and immunohistochemistry. Terminal deoxynucleotidyl transferase dUTP nick end labeling (TUNEL) and bromodeoxyuridine (BrdU) assays were performed to identify apoptotic and proliferating cells. Macroscopic observation of the *lag* mutant cerebellum reveals a marked reduction in size compared to wild-type mice. HE staining displays a normal foliation and lamination pattern in the *lag* mutant cerebellum, but detailed analysis has shown morphological disorganization in the cytoarchitectonics of the cerebellar cortex. The mutant internal granular layer is poorly defined and contains significantly fewer granule cells. Meanwhile, Purkinje cells form multilayer arrangements instead of a monolayer arrangement, as observed in wild-type mice, with their dendritic arborization being severely underdeveloped. Some Purkinje cells exhibit multiple nuclei, suggesting that the *Kif14* mutation disrupts normal cell division. These phenotypes are already recognized during early postnatal days, although no difference is determined before birth. TUNEL-positive cells are significantly more numerous in the mutant external granular layer, indicating that increased apoptotic cell death contributes to the diminished granule cell population in the *lag* mutant mouse. In conclusion, the *lag* mutant cerebellar cortex shows distinct structural abnormalities, suggesting that the *Kif14*-encoded protein exerts multifaceted roles in the development of the brain laminated structures as well as in myelin formation.

Keywords: *laggard*, *Kif14*, cerebellar cortex, granule cells, apoptosis

https://narraj.org/

Introduction

The cytoarchitectonics of the cerebellar cortex in mice is arranged into four well-defined layers: external granular layer (EGL), molecular layer (ML), Purkinje cell layer (PCL), and internal granular layer (IGL) [1]. This laminated structure develops during the perinatal period [2]. Numerous neuronal subtypes in the cerebellar cortex arise from two distinct germinal matrices: the ventricular germinal matrix and the rhombic lip [3]. Purkinje cells originate in the ventricular

Received: January 8, 2025 - Accepted: February 20, 2025 - Published online: April 21, 2025

germinal matrix and exit this region between embryonic days (E) 11 and E13 [4,5]. In contrast, cerebellar granule cells originate from a specialized germinal zone, known as the rhombic lip, between E13 and E15 [4,6]. Differently from Purkinje cells, granule cell precursors (GCPs) remain proliferative in the EGL until the end of the second postnatal week [5-7]. Starting in the EGL-the second proliferative zone-GCPs undertake a secondary inward migration along the vertical processes of Bergmann glia to create the IGL after birth [5,7]. Therefore, although GCPs arise prenatally, they exit the cell cycle and develop into mature granule cells postnatally, achieving their final numbers only after birth [8].

The *laggard* (*lag*) mutant mouse is a naturally arising mutant resulting from a splice site alteration in the *Kif14* gene [9]. Such a genetic alteration follows an autosomal recessive inheritance pattern. The *lag* mutant has severe cerebellar ataxia, begins losing weight significantly following the first week after birth, and experiences to early death around postnatal day (P) 14 [9]. Macroscopic examination reveals a noticeable reduction in the size of the central nervous system structures [10]. Moreover, brain-laminated structures, including the cerebellar cortex, cerebral cortex, hippocampus, and olfactory bulb, are significantly diminished relative compared to those in wild-type mice [9,10]. The *lag* mutant also exhibits pronounced hypomyelination of the brain and spinal cord, potentially resulting from impaired oligodendroglia maturation [9].

Kif14 is a mitotic kinesin motor protein essential for cytokinesis during cell division and is implicated in normal brain development [9-13]. *Kif14* facilitates proficient cytokinesis alongside citron kinase (citron-K) and protein regulator of cytokinesis 1 (PRC1) [14]. Disruption of these interactions can impair cell division and potentially trigger apoptosis [15]. In cells deficient in *Kif14*, citron-K fails to localize to the cleavage furrow region, thereby disrupting the maintenance of PRC1 at the midbody during mitosis [16]. The siRNA-intervened knockdown of *Kif14* leads to cytokinesis collapse, resulting in the development of binucleated cells, while partial knockdown of *Kif14* triggers programmed cell death after mitotic entry [17]. Mutations in *Kif14* in humans have been linked to a broad spectrum of phenotypes, varying from fetal death to mild developmental delays and microcephaly [18-21]. In comparison, *Kif14* overexpression has been closely linked to the development and progression of various cancers [22-24].

Despite *Kif14*'s substantial role in cytokinesis and cellular development, its specific involvement in cerebellar maturation remains unclear. The aim of this study was to investigate whether cerebellar maturation is affected in the *lag* mutant mouse, to describe the impact of the *Kif14* mutation on cerebellar development, and to provide insights into the mechanisms underlying *Kif14* function and its role in regulating cerebellar development.

Methods

Study design and setting

A comparative descriptive experimental study was conducted at the Division of Anatomy and Developmental Neurobiology, Kobe University Graduate School of Medicine, Kobe, Japan. This study's purpose was to examine the cytoarchitectural alterations in the developing cerebellar cortex of *lag* mutant mice, with a focus on the impact of *lag* mutation on cerebellar development. The study compared wild-type (+/+ or +/*lag*) and homozygous mutant (*lag*/*lag*) mice, all maintained on a C57BL/6J genetic background. Cellular organization and morphological changes in the cerebellum were evaluated, providing insights into developmental variations between the two mouse strains.

Animal preparation and eligibility

The entire group of wild-type (+/+ or +/*lag*) and homozygous mutant (*lag*/*lag*) mice were obtained through a controlled breeding population at the Institute for Experimental Animals, Kobe University Graduate School of Medicine, Kobe, Japan. Homozygous mutant mice (*lag/lag*) were generated by mating heterozygous carriers (+/*lag*) within the breeding colony at the age of 2–3 months. The genotypes of mice were confirmed using a polymerase chain reaction (PCR)-based genotyping process as described in a previous study [9]. Mice were included in the study based on their genotype, age, and developmental stage (both embryonic and postnatal days) to

ensure alignment with the study objectives. Offspring mice that died before the sacrifice process were excluded from the study.

Animal acclimatization and housing

In this study, all animals were acclimatized and housed under standardized conditions at the Institute for Experimental Animals, Kobe University Graduate School of Medicine, Kobe, Japan, to ensure consistency and animal well-being. The mice were housed in a cage measuring 29 cm (length) × 22 cm (width) × 14 cm (height), with a maximum of five adult mice per cage. Mating pairs, consisting of 1 male and 1–2 females, were placed in individual cages to facilitate controlled breeding. Pregnant females and lactating mothers, along with their offspring, were also housed in individual cages. The mice were kept under a 12-hour light-dark cycle with unrestricted access to food and water. The housing environment was maintained at a temperature of 20–26°C and a relative humidity of 30–70%.

Animal model

This study utilized wild-type (+/+ or +/*lag*) and homozygous mutant (*lag*/*lag*) mice to assess cytoarchitectural changes in the developing cerebellar cortex. The selection of time points for euthanasia was based on the developmental milestones of the cerebellar cortex and the viability constraints of the *lag* mutant mice, which typically did not survive beyond the second postnatal week. To examine the well-defined and mature cytoarchitectonics of the cerebellar cortex, euthanasia was performed at postnatal day (P) 10. To evaluate cytoarchitectural changes during prenatal and postnatal development, additional euthanasia time points included embryonic day (E) 17.5 and postnatal days (P) 0, P3, P5, and P7. For embryonic assessments, the presence of a vaginal plug in the morning following mating was designated as E0.5, as recommended previously [25]. A minimum of five mice per group was included at each developmental stage, ensuring reliability in histological observations, as recommended by the animal research: reporting of in vivo experiments (ARRIVE) guidelines [26]. By the end of the study, a total of 29 wild-type and 32 *lag* mutant mice were used.

Sample collection

Animals were deeply anesthetized using Somnopentyl, a barbiturate (5 mg/100 g body weight), via intraperitoneal injection to ensure minimal distress. Following sedation, transcardial perfusion was performed with 0.1 M phosphate-buffered saline (PBS) for 5 minutes at ambient temperature to clear blood from the vasculature. This was followed by perfusion with 4% paraformaldehyde (PFA) in 0.1 M phosphate buffer (PB) for 15 minutes at 4°C to achieve optimal fixation. Post-perfusion, the brains, extending to the upper cervical spinal cord, were carefully dissected to prevent structural damage. These samples were post-fixed in 4% PFA for 2 hours at 4°C to ensure uniform fixation and preservation of tissue architecture.

Hematoxylin-eosin (HE) staining and immunostaining

Fixed brain tissues were subjected to a dehydration process through an ascending ethanol gradient and subsequently cleared in xylene to remove lipids. The samples were embedded in paraffin wax to facilitate sectioning. Sagittal sections, 4 µm thick, were prepared using a precision sliding microtome SM2000R (Leica Biosystems, Wetzlar, Germany) and mounted onto MAS-coated glass slides (Matsunami Glass, Osaka, Japan) to ensure optimal adhesion. The sections underwent HE staining for histological examination. Briefly, sections were counterstained with hematoxylin, dehydrated through a graded ethanol series, cleared in xylene, and mounted using Harleco synthetic resin (HSR) solution (Sysmex, Kobe, Japan).

For immunostaining, paraffin-embedded sections adjacent to the HE-stained ones were rehydrated through a descending ethanol series and rinsed in 0.1 M PBS. Non-specific binding was minimized by incubating the sections in a blocking solution containing 0.1 M PBS and 1% bovine serum albumin for one hour. Primary antibody incubation was performed using anti-Calbindin (mouse monoclonal, Swant; 1:200 dilution), anti-glial fibrillary acidic protein (anti-GFAP) (rabbit polyclonal, Dako; 1:4 dilution), anti-myelin basic protein (anti-MBP) (rabbit polyclonal, Nichirei Biosciences; 1:1 dilution), and anti-S100B (mouse monoclonal, Abcam; 1:10

dilution). The incubation lasted one hour at room temperature, followed by overnight incubation at 4°C to enhance antigen-antibody binding.

The sections were washed three times in PBS, then incubated with biotinylated secondary antibodies: anti-mouse IgG or anti-rabbit IgG (Vector Laboratories; 1:500 dilution). Visualization was achieved using the avidin-biotin-peroxidase complex (ABC, Vector; 1:100 dilution) and subsequent development with 0.05% 3,3'-diaminobenzidine (DAB) and 0.01% hydrogen peroxide (H_2O_2) to produce a brown chromogenic reaction. Finally, the sections were rinsed in 0.1 M PBS, dehydrated through an ethanol gradient, cleared in xylene, and mounted with an HSR mounting medium.

Cytoarchitectonics of the cerebellar cortex

HE staining and immunohistochemistry were conducted to evaluate the cytoarchitectonics of the cerebellar cortex, a laminated brain structure consisting of four well-defined layers: EGL, ML, PCL, and IGL. The cytoarchitectonics in the P10 cerebellar cortex were representative of a well-defined and mature cerebellar cortex. Low-magnification HE staining was used to show the general appearance and foliation pattern of the cerebellum, while high-magnification HE staining was employed to observe the cytoarchitectonics of the cerebellar cortex. Cytoarchitectural changes in the developing cerebellar cortex were observed during both prenatal and postnatal periods. The cytoarchitectonics of the prenatal cerebellar cortex were observed at E17.5, while cytoarchitectural changes in the postnatal cerebellar cortex were periodically observed at P0, P3, P5, P7, and P10. Within this range, significant structural changes were already evident.

Immunostaining was used to identify specific neurons and neuroglia that contribute to the cytoarchitectonics of the cerebellar cortex. Anti-Calbindin staining highlighted Purkinje neurons, which predominantly form the PCL and its dendritic arborization. Anti-MBP staining identified myelinated nerve fibers in the white matter (WM). Anti-GFAP staining marked astrocytes, which were predominantly abundant in the PCL and IGL, including Bergmann glia in the PCL, whose vertical processes extended toward the EGL. Anti-S100B staining specifically highlighted the cell bodies of astrocytes.

Quantification of double-nucleated cells

To quantify the presence of double-nucleated Purkinje neurons in the *lag* mutant cerebellum, midsagittal sections of the vermis from P10 mice were analyzed. Cerebella from *lag* mutant (n=5) and wild-type (n=5) mice were paraffin-embedded and serially sectioned into 5 µm thick sagittal slices. The sample size was determined based on a power analysis, which estimated that a minimum of five animals per group would provide 80% power (β=0.2) to detect a biologically meaningful difference in the proportion of double-nucleated Purkinje neurons between wild-type and *lag* mutant mice at a significance level of α=0.05. This ensures statistical validity while minimizing animal use in accordance with ethical research guidelines. Sections were immunostained using an anti-Calbindin antibody to specifically label Purkinje neurons. The section passing through the cerebellar vermis midline was selected for analysis. All Calbindin-immunopositive Purkinje neurons within the section were examined using an Olympus AX80 microscope to identify those exhibiting double nuclei. Only neurons with clearly visible nuclear profiles were counted. However, the unadjusted counts were likely inflated, as nuclei may be divided across multiple sections during the slicing process [27]. To account for this, Abercrombie's correction factor was applied to adjust the raw counts [28]. This method accounts for nuclear diameter and ensures an accurate estimation of cell numbers. For correction factor calculation, nuclear diameters were measured from 50 randomly selected Calbindin-immunopositive Purkinje neurons per group. In wild-type mice, the mean nuclear diameter was 10.19 µm, while in *lag* mutants, it was 9.07 µm. Based on these values, the Abercrombie correction factors were determined as 0.33 for wild-type and 0.36 for *lag* mutant mice. The corrected quantification provided a more reliable representation of double-nucleated Purkinje neurons in both groups.

Terminal deoxynucleotidyl transferase dUTP nick end labeling (TUNEL) assay

Terminal deoxynucleotidyl transferase dUTP nick end labeling (TUNEL) assays were conducted using the DeadEnd Colorimetric TUNEL System (Promega, Madison, USA) following the

guidelines provided by the manufacturer. Paraffin-embedded tissue sections were cut into 5 µm slices, deparaffinized using xylene, and rehydrated through a graded ethanol series. The slides were then washed in 0.85% NaCl for 5 minutes, followed by washing in PBS. The slides were fixed in 4% PFA for 15 minutes at room temperature, treated with Proteinase K (20 µg/mL) for 15 minutes at room temperature, and washed again in PBS before being refixed in 4% PFA for 5 minutes at room temperature. The slides were covered with equilibration buffer provided in the kit and incubated with an rTdT reaction mix at 37°C for 60 minutes in a humidified chamber. The reaction was stopped using the provided stop buffer, followed by washing in PBS. To block the endogenous peroxidases activity, the slides were immersed in 0.3% hydrogen peroxide in PBS for 5 minutes at room temperature and then washed in PBS. Detection of biotin-labeled DNA ends was achieved by incubating the slides with streptavidin-conjugated horseradish peroxidase (HRP) for 30 minutes at room temperature. This was followed by the application of a DAB chromogenic substrate, resulting in a brown precipitate at sites of DNA fragmentation. The slides were dehydrated through a graded ethanol series, cleared with xylene, and coverslipped with a mounting medium. Apoptotic cells, identified by their brown-stained nuclei, were analyzed under a light microscope.

Bromodeoxyuridine (BrdU) labeling for assessment of cell proliferation and migration

To evaluate cell proliferation, bromodeoxyuridine (BrdU) was administered intraperitoneally at a dose of 10 mg per 100 g body weight to gestating mice at E17.5. Similarly, mouse pups at P10 received BrdU two hours prior to sacrifice. For cell migration assessment, pups at P10 were given two subcutaneous BrdU injections, two hours apart, followed by sacrifice three days later (P13). Embryos at E17.5 were fixed in 4% PFA for 12 hours before paraffin embedding. The brains of P10 and P13 pups were also harvested and prepared for paraffin embedding. Serial 4-µm-thick brain sections were prepared, with every fifth section subjected to 2 N HCl treatment for one hour at 37°C, followed by triple washing in PBS.

BrdU labeling was detected by incubating sections with an anti-BrdU antibody (BD Pharmingen, 1:500 dilution) for 24 hours at 4°C, followed by biotinylated anti-mouse IgG (Vector, 1:500 dilution) for one hour. The avidin-biotin-peroxidase complex was then applied for 30 minutes, and BrdU-reactive cells were visualized using a metal-enhanced diaminobenzidine (DAB) solution (0.025% $NiCl_2$; 0.025% $Co(CH_3COO)_2$; 0.05% 3,3'-DAB), resulting in dark blue or blue-black coloration. Sections were counterstained with nuclear fast red (Wako, Osaka, Japan).

Statistical analysis

Statistical analysis was conducted to evaluate differences in the corrected number of Calbindin-immunopositive Purkinje neurons between wild-type and *lag* mutant groups. Data were expressed as mean±SD. To determine statistical significance, the normality of the data was first assessed using the Shapiro-Wilk test. For normally distributed data, a two-tailed independent t-test was used to compare the corrected means of Calbindin-immunopositive Purkinje cells between groups. For non-normally distributed data, the Mann-Whitney U test was employed. All statistical analyses were carried out using SPSS version 24, (IBM, New York, US), with a significance level set at $p<0.05$.

Results

Cytoarchitectonics of the cerebellar cortex in P10 *lag* mutant mouse

The cerebellum of the P10 *lag* mutant mouse was diminished in overall dimensions relative to that of its wild-type littermate (**Figure 1A, A'**), as additionally demonstrated by low-magnification images of sagittal sections through P10 cerebellum (**Figure 1B, B'**). The mutant spinal cord and olfactory bulb exhibited a translucent appearance as a result of hypomyelination. In the mutant, cerebellar foliation appeared normal, as all major lobules were identifiable, although they were significantly smaller compared to the wild-type littermate (**Figure 1B, B'**). High-magnification images demonstrated normal lamination in the mutant cerebellar cortex,

although the ML and the IGL were strikingly reduced in layer thickness. Detailed analysis demonstrated that granule neurons in the mutant IGL were noticeably fewer than those in the wild-type littermate (**Figure 1C, C'**). The mutant Purkinje neurons were organized either in a zigzag pattern within a single layer or formed multiple cell layers rather than the single-layer arrangement observed in the wild-type littermate. The mutant EGL was less dense than the wild-type, and its deep border was more irregular.

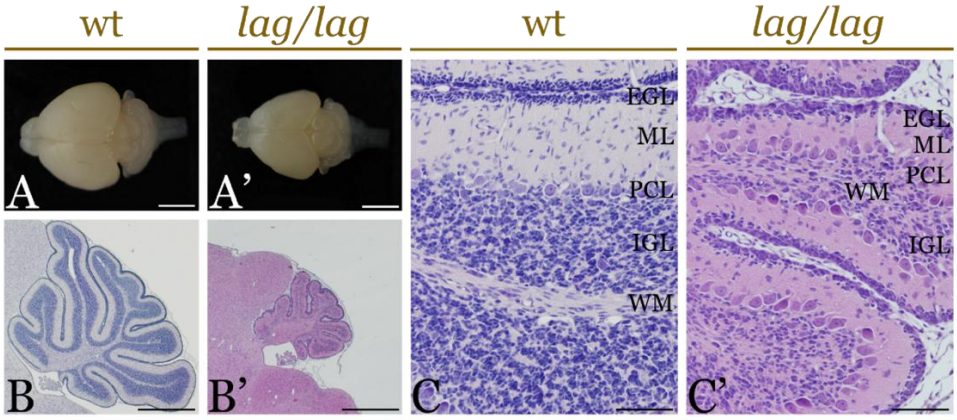

Figure 1. Dorsal surface view of the brains (A: wild-type; A': *lag* mutant) and HE-stained sagittal sections of the cerebella at P10, shown at low magnification (B: wild-type; B': *lag* mutant) and high magnification (C: wild-type; C': *lag* mutant). Scale bars: 3 mm (A, A'), 1 mm (B, B'), 100 µm (C, C'). EGL: external granular layer; IGL: internal granular layer; ML: molecular layer; PCL: Purkinje cell layer; WM: white matter; and wt: wild-type.

In both wild-type and *lag* mutant mice, the somata and dendritic projections of Purkinje neurons exhibited strong immunostaining with the anti-Calbindin antibody (**Figure 2A, A'**). Nevertheless, Calbindin-immunopositive Purkinje cells were arranged in a zigzag fashion or formed multiple cell layers rather than the single-cell arrangement observed in the wild-type littermate, and their dendritic arborization was severely underdeveloped in the *lag* mutant mouse. In addition, some dendritic processes of Purkinje cells penetrated through the EGL to reach beneath the pia mater. Some Calbindin-immunopositive Purkinje cells in this mutant had a large cell body (**Figure 2A', B**). Some of these Calbindin-immunopositive Purkinje cells had double nuclei in the large cell body (**Figure 2C**). Such double-nucleated Purkinje cells were also demonstrated by HE or cresyl violet staining (**Figure 2D, E**).

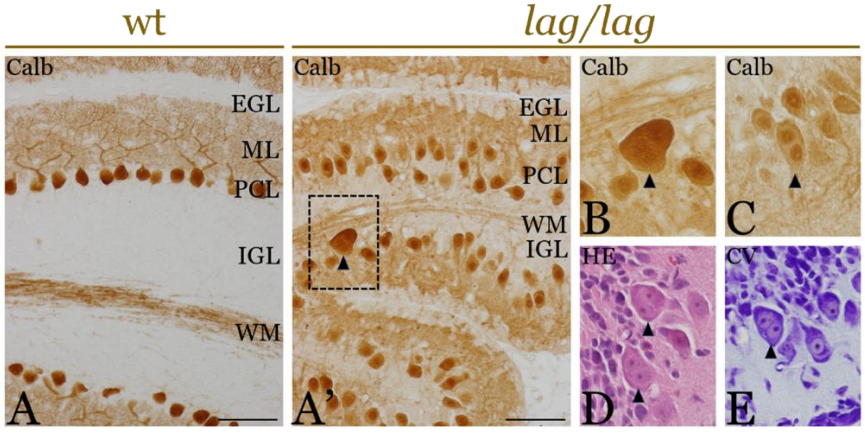

Figure 2. Calbindin expression in sagittal sections of the cerebella of wild-type (A) and *lag* mutant (A') mice at P10. Double-nucleated Purkinje neurons (arrowheads) are found in the *lag* mutant in Calbindin immunohistochemistry (B, high magnification of the Purkinje neuron shown in the inset in A'; C, Calbindin-immunopositive double-nucleated Purkinje neuron found in another section), HE-stained (D), and cresyl violet-stained (E) sections. Scale bars: 100 µm. Calb: Calbindin; CV: cresyl violet; EGL: external granular layer; HE: hematoxylin-eosin; IGL: internal granular layer; ML: molecular layer; PCL: Purkinje cell layer; WM: white matter; and wt: wild-type.

Subsequently, the total count of double-nucleated Calbindin-immunopositive Purkinje cells was determined from a median section of the P10 cerebellar vermis, presented in **Figure 3A**. Statistical analysis using an independent two-tailed t-test showed no significant difference in the mean number of Calbindin-immunopositive Purkinje cells per section between the two groups of mice (147±11 vs 154±10; p=0.39). However, the mean number of double-nucleated Calbindin-immunopositive Purkinje cells per section was significantly different between the two groups, with 1.83% of Calbindin-immunopositive Purkinje cells exhibiting double nuclei in *lag* mutant mice (0 vs 3±1; p=0.003), a feature not observed in the wild-type group. These findings indicate that aberrant cell division arises in the mutant cerebellum.

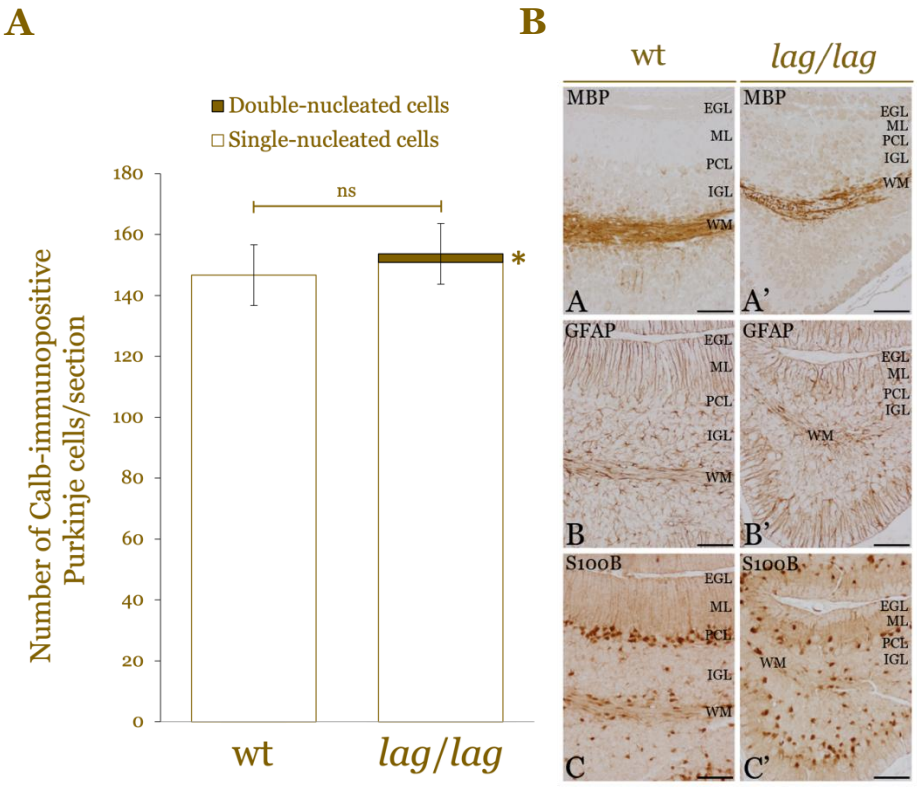

Figure 3. Comparison of Calbindin-immunopositive Purkinje cells and the expression of macroglial markers between wild-type and *lag* mutant mice at P10. Panel A: Comparison of Calbindin-immunopositive Purkinje cells between wild-type and *lag* mutant mice at P10. ns: not significant (p>0.05); *statistically significant (p<0.05). Panel B: Expression of MBP (A: wild-type; A': *lag* mutant), GFAP (B: wild-type; B': *lag* mutant), and S100B (C: wild-type; C': *lag* mutant) in sagittal sections of the cerebella at P10. Scale bars: 100 µm. EGL: external granular layer; IGL: internal granular layer; ML: molecular layer; PCL: Purkinje cell layer; WM: white matter; and wt: wild-type.

In both P10 wild-type and *lag* mutant cerebellar cortices, MBP-reactive myelinated nerve fibers were identified across the WM. However, MBP-immunopositive axons were slightly decreased and appeared coarse in the mutant (**Figure 3B**). GFAP-immunoreactivity was not notably different between both mice. However, the palisade arrangement of GFAP-immunopositive Bergmann glial processes in the *lag* mutant ML was shorter and more irregular than the wild-type (**Figure 3B**). Next, immunohistochemical staining using anti-S100B antibody was conducted to stain cell bodies of astrocytes. Interestingly, the count of S100B-immunopositive Bergmann glia was reduced in the mutant and appeared more widely dispersed across both the ML and PCL (**Figure 3B**).

Cytoarchitectural changes in the *lag* mutant cerebellar cortex during prenatal and postnatal development

Subsequently, the cytoarchitectural changes in the cerebellar cortex of the reference strain and *lag* mutant mice were examined during prenatal and postnatal development. During the prenatal

period, the cerebellum size was comparable between wild-type and *lag* mutant mice (data not shown). Moreover, no significant difference in the cerebellar cytoarchitectonics could be identified between both mice during prenatal days. After birth, the normal cerebellum size increased with age, reaching its mature size by P10. In contrast, the mutant cerebellum exhibited no significant growth during the postnatal period (**Figure 4A-E, A'-E'**), resulting in its smaller size at P10.

In both wild-type and *lag* mutant mice, every laminar structure of the cerebellar cortex was identifiable from P0 to P10 (**Figure 4A"-E", A"'-E"'**). In the mutant, Purkinje cells were organized in a zigzag pattern or formed multiple cell layers rather than the single-layered structure observed in the wild-type cerebellar cortex. The concentration of granule neurons in the mutant EGL was found to be lower than that of the wild-type during postnatal development. Similarly, the number of granule cells in the mutant IGL was reduced and continued to decline throughout the postnatal period (**Figure 4A"'-E"'**).

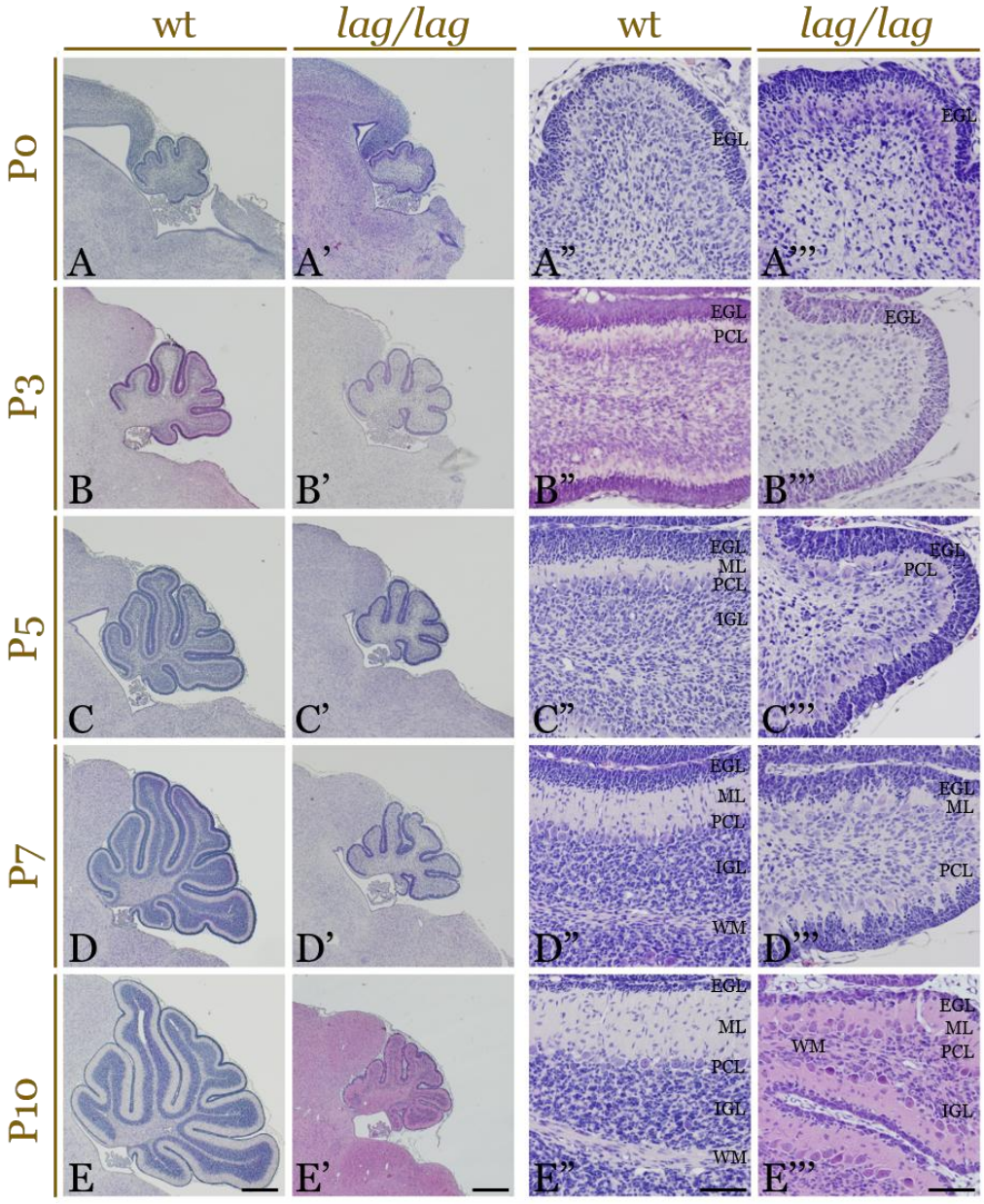

Figure 4. Postnatal developmental changes in the cytoarchitectonics of the cerebella of wild-type and *lag* mutant mice at different stages, shown at low magnification (A-E: wild-type; A'-E': *lag* mutant) and high magnification (A"-E": wild-type; A"'-E"': *lag* mutant) in sagittal sections. Scale bars: 1 mm (A-E, A'-E'), 100 µm (A"-E", A"'-E"'). EGL: external granular layer; IGL: internal granular layer; ML: molecular layer; PCL: Purkinje cell layer; WM: white matter; and wt: wild-type.

Next, Calbindin immunohistochemistry was performed to contrast the developmental progression of Purkinje cells during the postnatal period. Calbindin-immunopositive Purkinje cells were labeled in the PCL of the cerebellar cortex both in the wild-type and *lag* mutant mice during postnatal days. During the early postnatal days, no differences were observed in the distribution of Calbindin-immunopositive Purkinje cells between wild-type and *lag* mutant mice. However, after P5, the Calbindin-immunopositive Purkinje cells in the mutant cerebellar cortex were arranged in a zigzag pattern or formed multiple cell layers, differing from the single-layer configuration observed in the wild-type (**Figure 5A-C, A'-C'**). The dendritic branching of Purkinje cells was distinctly evident in the wild-type mice at P7 and P10 (**Figure 5B, C**), whereas it appeared ill-defined in the *lag* mutant mouse (**Figure 5B', C'**). Some mutant Calbindin-immunopositive Purkinje neurons had enlarged somas than those of wild-type cells, as previously noted. Furthermore, a small number of these Calbindin-immunopositive Purkinje cells displayed double nuclei (**Figure 5C'**).

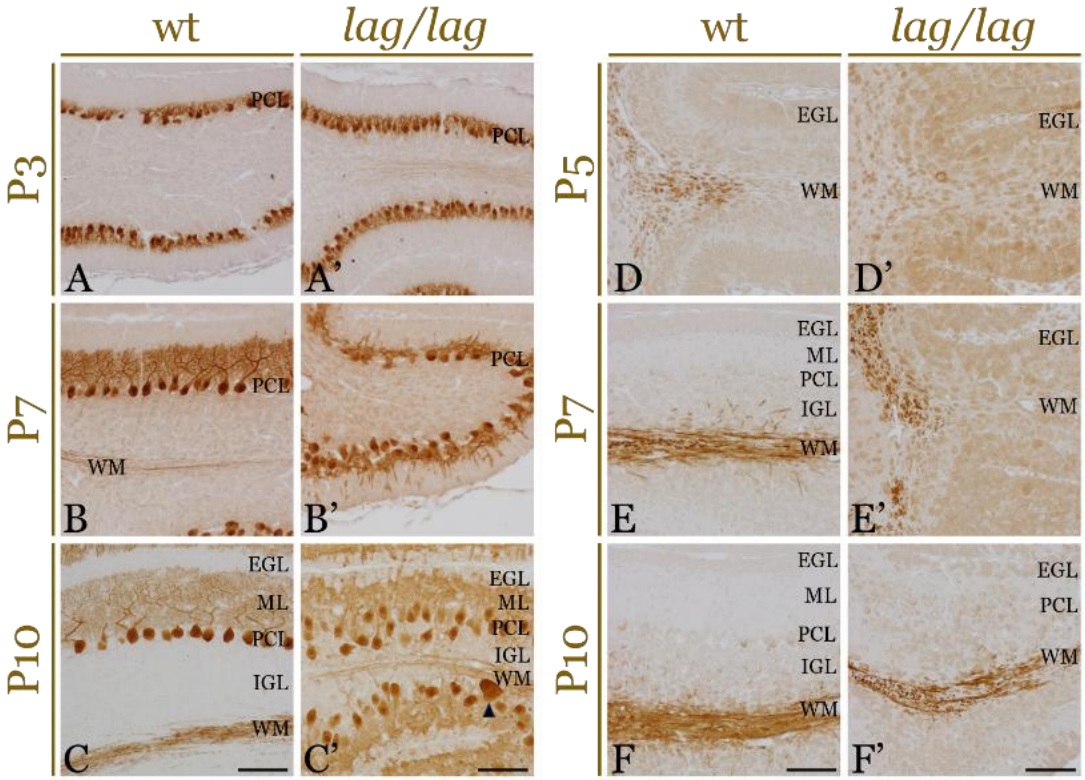

Figure 5. Postnatal developmental changes in the Calbindin (A-C: wild-type; A'-C': *lag* mutant) and MBP (D-F: wild-type; D'-F': *lag* mutant) expressions of the cerebella at different stages in sagittal sections. Calbindin-immunopositive double-nucleated Purkinje neuron (arrowhead) is found in the *lag* mutant mice at P10. Scale bars: 100 µm. EGL: external granular layer; IGL: internal granular layer; ML: molecular layer; PCL: Purkinje cell layer; WM: white matter; and wt: wild-type.

To compare the developmental changes of the glial cells in the cerebellar cortex, MBP-, GFAP-, and S100B-immunohistochemistries were conducted. MBP-reactive myelinated nerve fibers in the normal cerebellar cortex were dispersed within the WM at P5 (**Figure 5D**). However, MBP-immunoreactive myelin-sheathed fibers were absent in the mutant white matter until P7 (**Figure 5E'**). The distribution pattern of MBP-immunopositive fibers was comparatively similar between P5 wild-type and P7 mutant (**Figure 5D, E'**) as well as P7 wild-type and P10 mutant cerebella (**Figure 5E, F'**), indicating a delayed maturation of oligodendrocyte and myelin formation in the *lag* mutant mouse. GFAP- and S100B-immunoreactivity and distribution patterns of GFAP- and S100B-immunopositive cells were not notably different between both mice during early postnatal days (**Figure 6A, A', D, D'**). During the late postnatal days, the palisade arrangement of GFAP-immunopositive Bergmann glial processes appeared more irregular in the mutant mouse (**Figure 6B, B', C, C'**). Additionally, S100B-immunopositive Bergmann glial cells

in the mutant were reduced in number and more widely dispersed across both the ML and PCL compared to the wild-type littermate (**Figure 6E, E', F, F'**).

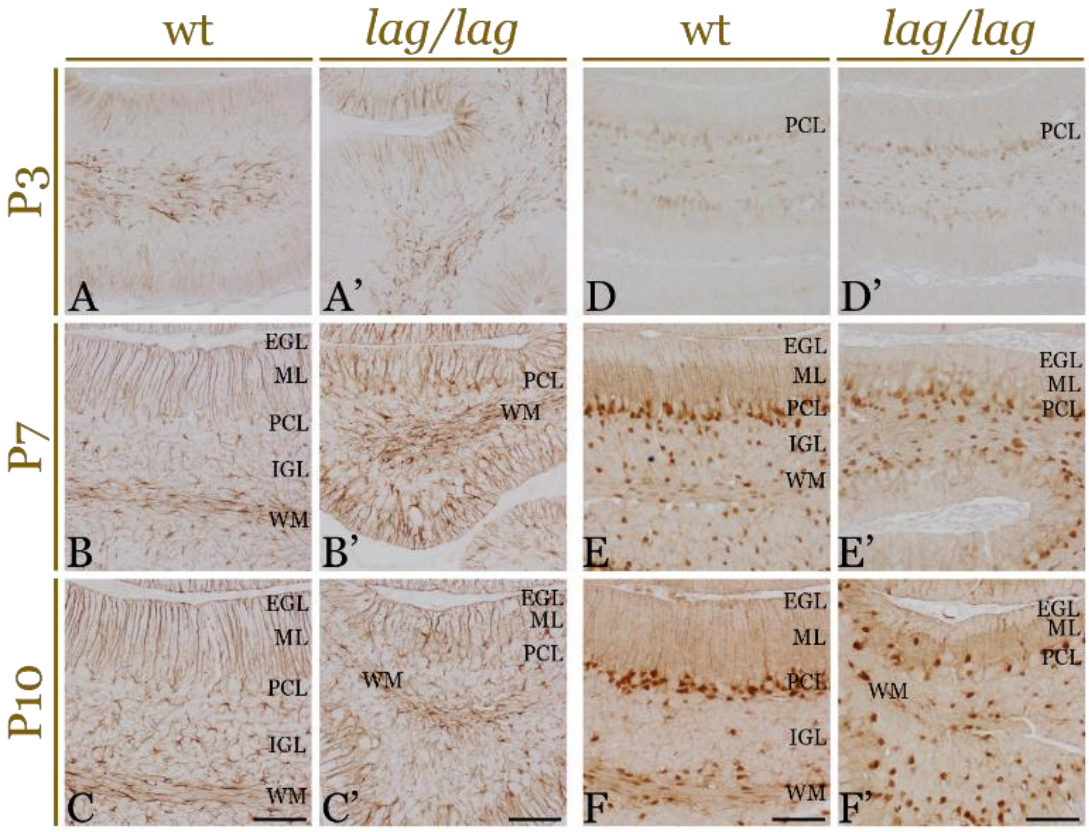

Figure 6. Postnatal developmental changes in the GFAP (A-C: wild-type; A'-C': *lag* mutant) and S100B (D-F: wild-type; D'-F': *lag* mutant) expressions of the cerebella at different stages in sagittal sections. Scale bars: 100 µm. EGL: external granular layer; IGL: internal granular layer; ML: molecular layer; PCL: Purkinje cell layer; WM: white matter; and wt: wild-type.

TUNEL and BrdU assays

Neural development is governed by the equilibrium between cellular growth and programmed cell death during normal brain maturation. The reduced cellularity discovered in the *lag* mutant cerebellum may result from either a decrease in cell proliferation, an increase in cell death (apoptosis), or a combination of both. Apoptotic cells were specifically labeled using the TUNEL assay to assess an increase in cell death. A higher number of TUNEL-stained neurons were detected within the deep zone of the mutant EGL compared to the wild-type littermate during the postnatal period, particularly at P10, suggesting a significant apoptotic activity (**Figure 7A-D, A'-D'**). In contrast, although the *lag* mutant mouse exhibited reduced cellularity, the concentration and arrangement of BrdU-reactive cells during prenatal ages did not differ significantly between the wild-type and mutant mice (**Figure 7E, E'**). At P10, BrdU-positive cells were predominantly localized to the superficial zone of the EGL in wild-type mice, whereas in the mutant, these cells were more widely dispersed throughout the EGL (**Figure 7F, F'**). To evaluate potential migration defects, BrdU was injected at P10, and the mice were sacrificed three days later. BrdU-stained neurons were primarily detected in the EGL and IGL of both wild-type and *lag* mutant mice; nevertheless, BrdU immunostaining was slightly reduced in the *lag* mutant mouse (**Figure 7G, G'**). These results indicate apoptotic cells in the deep zone of the mutant EGL were caused by cytokinesis failure instead of migration defect.

Yunus et al. Narra J 2025; 5 (2): e2075 - http://doi.org/10.52225/narra.v5i2.2075

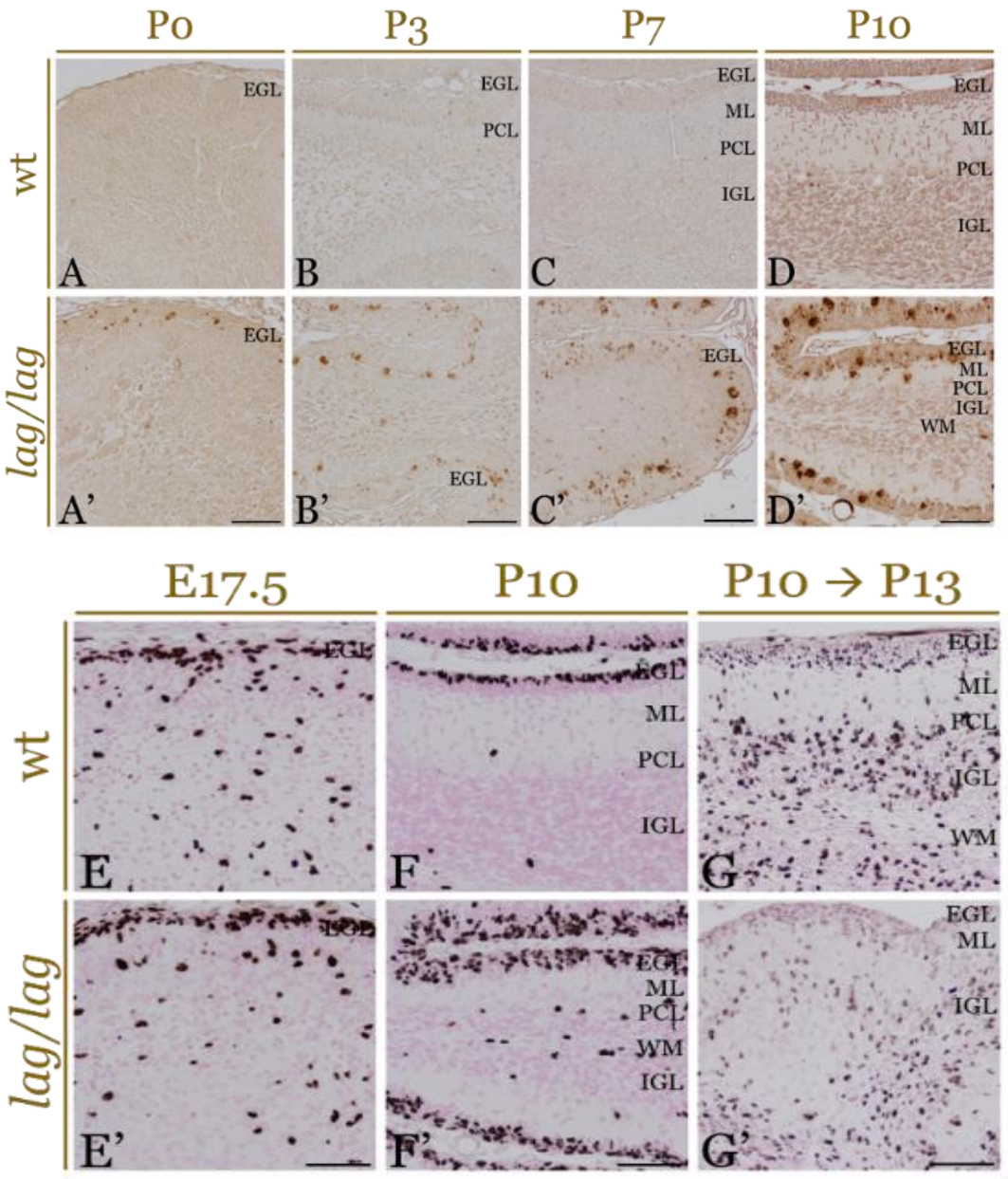

Figure 7. TUNEL assay during the postnatal period (A-D: wild-type; A'-D': *lag* mutant) and BrdU assay during the prenatal and postnatal periods (E-G: wild-type; E'-G': *lag* mutant) in sagittal sections of the cerebella from both groups. Scale bars: 100 µm. EGL: external granular layer; IGL: internal granular layer; ML: molecular layer; PCL: Purkinje cell layer; WM: white matter; and wt: wild-type.

Discussion

The present study has demonstrated that granule cells in the IGL of the P10 *lag* mutant cerebellar cortex are dramatically reduced compared to those in the wild-type littermate, giving a sparse appearance to the mutant IGL (**Figure 1C'**). In the mutant, the decreased granule cell density in the IGL was already identified at P0 and continued to decrease with age until P10 (**Figure 4**). The cell density in the mutant EGL was almost similar to the wild-type during early postnatal days, although the border between the deep zone of the EGL and the ML in the mutant was ill-defined after P5 (**Figure 4C'''**). The present TUNEL assay has revealed that extensive cell death occurs in the deep zone of the EGL during the postnatal period, starting from P0 and continuing through P10 in the mutant. In contrast, no apoptotic cells are identified in the wild-type (**Figure 7A-D**), implying that the number of postmitotic granule neurons in the deep zone of the mutant EGL prior to inward migration was reduced. Conversely, the present BrdU assay has shown that no notable deficits in proliferation within the EGL of the *lag* mutant mouse during both prenatal

and postnatal periods (**Figure 7E', F'**). Although there was substantial granule cell loss in the IGL, the inward migration of granule cells along the radial processes of Bergmann glial cells [29,30] appears to remain intact, as presented by the 3-day BrdU assay in this study (**Figure 7G'**). These results strongly indicate that granule cell progenitors in the second proliferative zone, specifically the superficial zone of the EGL, undergo cytokinesis failure. This failure triggers apoptosis of postmitotic granule cells in the deep zone of the EGL, ultimately leading to reduced granule cell density in the IGL [31]. The phenotypes exhibited by the *lag* mutant mouse closely resemble those seen in the citron-K amorphic mutant [32,33].

This quantitative analysis has indicated that the number of Purkinje cells was almost identical to the wild-type littermate (**Figure 3A**). The unaltered number of Purkinje cells may be attributed to the fact that most Purkinje cells are generated between E11 and E13, prior to the peak expression of *Kif14* (E12.5–16.5) [9,31]. However, the present Calbindin immunohistochemistry, HE, and cresyl violet staining have revealed that only a small number of Purkinje cells possess a sizable cell body and are occasionally double-nucleated (**Figure 2B-E**). These double-nucleated Purkinje cells with a large cell body can survive, migrate to their final settlement, and differentiate [34]. However, they are distributed in a zigzag fashion or form multiple cell layers between the thin ML and the IGL, and their dendritic arborizations are severely underdeveloped. Our previous study revealed that some mitral cells in the mitral cell layer of the *lag* olfactory bulb are also double-nucleated [10]. A study in 2011 reported that multinucleated neurons in citron-K deficient rats were capable of migrating to the appropriate layers of the cerebral neocortex, similar to the behavior observed in Purkinje cells and mitral cells of the *lag* mutant mouse [34]. The multinucleated cells in the citron-K mutant exhibit an increased quantity of cilia, indicating ineffective cytokinesis resulting from the lack of citron-K [34]. Combined with previous and present studies, double-nucleated neurons with an enlarged cell body in *lag* mutant mice are capable of migrating from their site of origin to their final destination.

As described above, the phenotypes observed in the *lag* mutant mouse closely resemble the characteristics of the citron-K amorphic mutant mouse [31] and rat [8,34]. In both the citron-K amorphic mutant mouse and rat, the cerebral cortex, cerebellar cortex, and olfactory bulbs are significantly diminished in dimensions, as observed in the *lag* mutant mouse. Additionally, the counts of olfactory granule neurons and cerebellar granule neurons are substantially diminished in both citron-K amorphic mutant models, and mitral cells and Purkinje cells are sporadically double-nucleated in the citron-K deficient rat [31,34]. Our prior study revealed that *Kif14* was strongly expressed during the E12.5–16.5 developmental period, which aligns with the expression timeline of citron-K [9,31]. Although *Kif14* and citron-K are not necessary for the formation of the central spindle and cytokinetic groove (cleavage furrow) during initial cytokinesis or the cytokinetic bridge (midbody) during final-stage cytokinesis, the pair is crucial for ensuring proficient cytokinesis [14]. *Kif14* has been observed to concentrate at the central spindle and cytokinetic bridge during cytokinesis [35]. Furthermore, citron-K is necessary for the positioning of *Kif14* at the cytokinetic bridge, in addition to the existence of PRC1 [36]. At the same time, *Kif14* is essential for the positioning of citron-K at the cytokinetic bridge and for its role in cytokinesis [14,16]. In cells lacking *Kif14*, citron-K is lost from the central spindle and cytokinetic groove area [14]. When citron-K is depleted, it disrupts the stability of the cytokinetic bridge during middle to late stages of telophase and the preservation of PRC1 in the cytokinetic bridge during final-stage telophase, ultimately leading to cytokinesis collapse concurrent with midbody formation or in the subsequent stage [14,16].

A prior study in 2001 showed that the citron-K gene mutation is time-sensitive, with its effects confined to a specific period (between E16 and birth in rats) [32]. Nerve cells produced before the onset of the mutation (E16 in the rat) and the cells that endure the mutation are capable of undergoing normal differentiation [32]. During mouse cerebellar development, the majority of Purkinje neurons are formed between E11 and E13, while granule neurons are predominantly produced from late embryonic stages (approximately E15) to postnatal day 15 (P15) [4]. This neurogenesis timeline for primary cerebellar neurons aligns with the timing of *Kif14* and citron-K expression, which peak throughout the subsequent phases of neural maturation [9,31]. Consequently, mutations in these genes have a more pronounced impact on neurons formed

during late neurogenesis, such as cerebellar granule cells [37]. In the CNS, although citron-K is exclusively manifested in dividing neural progenitors, only a specific group of these progenitors depends on citron-K to effectively finalize cell separation [31]. The neuronal populations most affected by citron-K depletion include granule and periglomerular neurons in the olfactory bulb, as well as granule neurons in the dentate gyrus of the hippocampus and the cerebellar cortex [31]. These neurons originate from secondary neurogenic regions and exhibit similar physiological, morphological, and biochemical characteristics [31,38].

While the precise mechanisms behind hypomyelination are still unclear, our prior studies indicate that inadequate myelination in the *lag* mutant mouse results from impaired oligodendrocyte maturation [9,10], as demonstrated by MBP immunostaining (**Figure 5D'-F'**). Furthermore, our current findings revealed that GFAP immunoreactivity exhibits no notable difference between *lag* mutant and wild-type mice. However, the number of S100B-immunopositive cells is reduced in the mutant compared to wild-type littermates during late postnatal stages (**Figure 6E', F'**). As S100B expression is associated with astrocyte maturation, the reduced S100B-immunopositivity may indicate a failure of immature astrocytes to fully differentiate into mature astrocytes. Following our previous studies [9,10], our findings imply that the *Kif14* alteration could interfere with the maturation process of neuroglia. These observations suggest that the *Kif14* mutation likely does not impact the generation or differentiation of glial cells but instead interferes with their maturation. In citron-K amorphic mutant rats, GFAP immunolabeling fails to detect a substantial quantity of binucleated cells [32,39]. The timing of citron-K expression, which closely parallels that of *Kif14* around birth, highlights its crucial role in facilitating proper cytokinesis in certain neurons produced during embryonic and postnatal periods. However, citron-K appears to play a less critical role in glial cells, despite the fact that most gliogenic cell divisions take place during the postnatal period [39]. From prior and current findings, neither *Kif14* nor citron-K is directly involved in the generation or specialization of neuroglia in the cerebellum. Nevertheless, the *Kif14* mutation might interfere with the normal development process of neuroglia.

Conclusion

This study revealed significant developmental disruptions caused by the *lag* mutation. Despite preserved cortical lamination, abnormalities were observed, including double-nucleated Purkinje neurons, altered astrocytic distributions, and increased apoptosis, predominantly in granule cells. The elevated granule cell apoptosis, identified through TUNEL assays, suggests impaired survival mechanisms contributing to cerebellar cytoarchitectural abnormalities. In addition, the underlying mechanism of disrupted myelin formation in the *lag* mutant mouse remains unresolved. Currently, no evidence suggests that *Kif14* directly influences oligodendrocyte maturation or myelination. Further studies are necessary to clarify the specific contributions of *Kif14* in oligodendrocyte maturation and myelin formation. These findings provide insights into the molecular and cellular effects of the *Kif14* mutation and its role in cerebellar disorders, offering a foundation for future research into neurodevelopmental abnormalities.

Ethics approval

All procedures adhered to the National Institute of Health Guide for the Care and Use of Laboratory Animals (NIH Publications No. 80-23), revised in 1996, and were approved by the Committee on Animal Care and Welfare, Kobe University Graduate School of Medicine.

Acknowledgments

Gratitude is extended to all members of the Division of Anatomy and Developmental Neurobiology (Kobe University Graduate School of Medicine).

Competing interests

All the authors declare that there are no conflicts of interest.

Funding

This study was funded by Grants-in-Aid from the Ministry of Education, Culture, Sports, Science, and Technology (No. 20300119, 24300126, 24650177 to Toshio Terashima). The funding agency had no contribution in the design or implementation of the study.

Underlying data

The datasets generated or analyzed during this study are incorporated in the submission. Derived data supporting the findings of this study are accessible from the corresponding author on request.

Declaration of artificial intelligence use

This study used artificial intelligence (AI) tools and methodologies in the following capacities: AI-based language model, ChatGPT, was employed for language refinement (improving grammar, sentence structure, and readability of the manuscript). We confirm that all AI-assisted processes were critically reviewed by the authors to ensure the integrity and reliability of the results. The final decisions and interpretations presented in this article were solely made by the authors.

How to cite

Yunus J, Setsu T, Kikkawa S, Terashima T. Cytoarchitectural changes in the developing cerebellar cortex of the *laggard* mutant mouse. Narra J 2025; 5 (2): e2075 - http://doi.org/10.52225/narra.v5i2.2075.

References

1. Sillitoe R V., Fu Y, Watson C. Cerebellum. In: Watson C, Paxinos G, Puelles L, editors. The mouse nervous system. London: Academic Press; 2012.
2. Hibi M, Shimizu T. Development of the cerebellum and cerebellar neural circuits. Dev Neurobiol 2012;72:282-301.
3. Wang VY, Zoghbi HY. Genetic regulation of cerebellar development. Nat Rev Neurosci 2001;2(7):484-491.
4. Miale IL, Sidman RL. An autoradiographic analysis of histogenesis in the mouse cerebellum. Exp Neurol 1961;4:277-296.
5. Goldowitz D, Hamre K. The cells and molecules that make a cerebellum. Trends Neurosci 1998;21(9):375-382.
6. Alder J, Cho NK, Hatten ME. Embryonic precursor cells from the rhombic lip are specified to a cerebellar granule neuron identity. Neuron 1996;17(3):389-399.
7. Hatten ME, Mason C A. Mechanisms of glial-guided neuronal migration in vitro and in vivo. Experientia 1990;46(9):907-916.
8. Roberts MR, Bittman K, Li WW, *et al.* The flathead mutation causes CNS-specific developmental abnormalities and apoptosis. J Neurosci 2000;20(6):2295-2306.
9. Fujikura K, Setsu T, Tanigaki K, *et al. Kif14* mutation causes severe brain malformation and hypomyelination. PLoS One 2013;8(1):e53490.
10. Yunus J, Setsu T, Kikkawa S, *et al.* Cytoarchitecture of the olfactory bulb in the *laggard* mutant mouse. Neuroscience 2014;275:259-271.
11. Nakagawa T, Tanaka Y, Matsuoka E, *et al.* Identification and classification of 16 new kinesin superfamily (KIF) proteins in mouse genome. Proc Natl Acad Sci U S A 1997;94(18):9654-9659.
12. Miki H, Setou M, Kaneshiro K, *et al.* All kinesin superfamily protein, KIF, genes in mouse and human. Proc Natl Acad Sci U S A 2001;98(13):7004-7011.
13. Arora K, Talje L, Asenjo AB, *et al. Kif14* binds tightly to microtubules and adopts a rigor-like conformation. J Mol Biol 2014;426(17):2997-3015.
14. Gruneberg U, Neef R, Li X, *et al. Kif14* and citron kinase act together to promote efficient cytokinesis. J Cell Biol 2006;172(3):363-372.
15. Basavarajappa HD, Corson TW. *Kif14* as an oncogene in retinoblastoma: A target for novel therapeutics? Future Med Chem 2012;4(17):2149-2152.
16. Watanabe S, De Zan T, Ishizaki T, *et al.* Citron kinase mediates transition from constriction to abscission through its coiled-coil domain. J Cell Sci 2013;126(Pt 8):1773-1784.

17. Carleton M, Mao M, Biery M, *et al.* rna interference-mediated silencing of mitotic kinesin *Kif14* disrupts cell cycle progression and induces cytokinesis failure. Mol Cell Biol 2006;26(10):3853-3863.
18. Filges I, Nosova E, Bruder E, *et al.* Exome sequencing identifies mutations in *Kif14* as a novel cause of an autosomal recessive lethal fetal ciliopathy phenotype. Clin Genet 2014;86(3):220-228.
19. Moawia A, Shaheen R, Rasool S, *et al.* Mutations of *Kif14* cause primary microcephaly by impairing cytokinesis. Ann Neurol 2017;82(4):562-577.
20. Makrythanasis P, Maroofian R, Stray-Pedersen A, *et al.* Biallelic variants in *Kif14* cause intellectual disability with microcephaly. Eur J Hum Genet 2018;26(3):330-339.
21. Reilly ML, Stokman MF, Magry V, *et al.* Loss of function mutations in *Kif14* cause severe microcephaly and kidney development defects in humans and zebrafish. Hum Mol Genet 2018;28(5):778-795.
22. Jiang W, Wang J, Yang X, *et al. Kif14* promotes proliferation, lymphatic metastasis and chemoresistance through G3BP1/YBX1 mediated NF-κB pathway in cholangiocarcinoma. Oncogene 2023;42(17):1392-1404.
23. Wang H, Tang F, Tang P, *et al.* Noncoding RNAs-mediated overexpression of *Kif14* is associated with tumor immune infiltration and unfavorable prognosis in lung adenocarcinoma. Aging 2022;14(19):8013-8031.
24. Zhang J, Buranjiang G, Mutalifu Z, *et al. Kif14* affects cell cycle arrest and cell viability in cervical cancer by regulating the p27Kip1 pathway. World J Surg Oncol 2022;20(1):125.
25. Heyne GW, Plisch EH, Melberg CG, *et al.* A simple and reliable method for early pregnancy detection in inbred mice. J Am Assoc Lab Anim Sci 2015;54(4):368-371.
26. Kilkenny C, Browne WJ, Cuthill IC, *et al.* Improving bioscience research reporting: The arrive guidelines for reporting animal research. PLoS Biol 2010;8(6):e1000412.
27. Konigsmark BW. Methods for the counting of neurons. In: Nauta wjh, ebbesson soe, editors. Contemporary research methods in neuroanatomy. Berlin: Springer Berlin Heidelberg; 1970.
28. Abercrombie M. Estimation of nuclear population from microtome sections. Anat Rec 1946;94:239-247.
29. Jakovcevski I, Siering J, Hargus G, *et al.* Close homologue of adhesion molecule L1 promotes survival of purkinje and granule cells and granule cell migration during murine cerebellar development. J Comp Neurol 2009;513(5):496-510.
30. Basille-Dugay M, Hamza MM, Tassery C, *et al.* Spatio-temporal characterization of the pleiotrophinergic system in mouse cerebellum: Evidence for its key role during ontogenesis. Exp Neurol 2013;247:537-551.
31. Di Cunto F, Imarisio S, Hirsch E, *et al.* Defective neurogenesis in citron kinase knockout mice by altered cytokinesis and massive apoptosis. Neuron 2000;28(1):115-127.
32. Mitchell BD, Gibbons B, Allen LR, *et al.* Aberrant apoptosis in the neurological mutant Flathead is associated with defective cytokinesis of neural progenitor cells. Brain Res Dev Brain Res 2001;130(1):53-63.
33. Ackman JB, Ramos RL, Sarkisian MR, *et al.* Citron kinase is required for postnatal neurogenesis in the hippocampus. Dev Neurosci 2007;29(1–2):113-123.
34. Anastas SB, Mueller D, Semple-Rowland SL, *et al.* Failed cytokinesis of neural progenitors in citron kinase-deficient rats leads to multiciliated neurons. Cereb Cortex 2011;21(2):338-344.
35. Cai S, Weaver LN, Ems-McClung SC, *et al.* Proper organization of microtubule minus ends is needed for midzone stability and cytokinesis. Curr Biol 2010;20(9):880-885.
36. Bassi ZI, Audusseau M, Riparbelli MG, *et al.* Citron kinase controls a molecular network required for midbody formation in cytokinesis. Proc Natl Acad Sci U S A 2013;110(24):9782-9787.
37. Chizhikov V V., Millen KJ. Neurogenesis in the cerebellum. In: Rubenstein J, Rakic P, Chen B, Kwan KY, editors. Patterning and cell type specification in the developing cns and pns. London: Academic Press; 2020.
38. Hatten ME, Alder J, Zimmerman K, *et al.* Genes involved in cerebellar cell specification and differentiation. Curr Opin Neurobiol 1997;7(1):40-47.
39. LoTurco JJ, Sarkisian MR, Cosker L, *et al.* Citron kinase is a regulator of mitosis and neurogenic cytokinesis in the neocortical ventricular zone. Cereb Cortex 2003;13(6):588-591.